Le Friant, A., Ishizuka, O., Stroncik, N.A., and the Expedition 340 Scientists
Proceedings of the Integrated Ocean Drilling Program Volume 340
publications.iodp.org

Data report: permeability measurements inside and outside submarine landslides at IODP Expedition 340 sites[1]

L. Koehn,[2,3] T. Kyritz,[2,3] M. Hornbach,[2] J. Berry,[2] P. Betz,[2] M. White,[2] A. Martinez,[2] J.M. Martinez-Camacho,[2] C. McCracken,[2] J. Renzaglia,[2] J. Sylvester,[2] and T. O'Toole[2]

[1] Koehn, L., Kyritz, T., Hornbach, M., Berry, J., Betz, P., White, M., Martinez, A., Martinez-Camacho, J.M., McCracken, C., Renzaglia, J., Sylvester, J., and O'Toole, T., 2022. Data report: permeability measurements inside and outside submarine landslides at IODP Expedition 340 sites. In Le Friant, A., Ishizuka, O., Stroncik, N.A., and the Expedition 340 Scientists, Proceedings of the Integrated Ocean Drilling Program, 340: Tokyo (Integrated Ocean Drilling Program Management International, Inc.). https://doi.org/10.2204/iodp.proc.340.208.2022
[2] Department of Earth Sciences, Southern Methodist University, USA. Correspondence author: **larskoehn@yahoo.com**
[3] Primary authors.

Keywords
Integrated Ocean Drilling Program, IODP, *JOIDES Resolution*, Expedition 340, Lesser Antilles Volcanism and Landslides, Site U1393, Site U1394, Site U1395, Site U1397, Site U1398, Site U1399

References (RIS)

MS 340-208
Received 3 May 2021
Accepted 13 January 2022
Published 29 March 2022

Abstract

Permeability data are fundamental to understanding subsurface fluid flow, fluid pressure, and subsequently submarine slope stability. Currently, few detailed permeability measurements exist in sediments that have undergone submarine slope failures. Here, we measure sediment permeability using the falling head method on samples obtained both within and adjacent to underwater slope failure deposits and from undisturbed sediment above and below these deposits collected during Integrated Ocean Drilling Program Expedition 340 in the Lesser Antilles island arc. Past studies of this volcanic island arc have identified several submarine landslide units created by volcanic slope collapse offshore the islands of Martinique and Montserrat, and two reports have been published on the permeabilities of clay-rich sediments from the slide units offshore Martinique. We measured sediment permeability in a greater range of samples, including volcaniclastic turbidites and hemipelagic muds from slope failure units offshore both Martinique and Montserrat. Results show permeability ranging from 4.27×10^{-11} to 9.14×10^{-15} m^2, and volcaniclastic sediments in slope deposits have the highest permeabilities. These results can be used to test hypotheses addressing permeability and fluid flow in submarine landslides containing hemipelagic sediment, and future integration of these measurements with time-dependent pore pressure models will ultimately enhance understanding of submarine slope stability.

1. Introduction

Submarine mass transport deposits such as those caused by volcanic island flank collapses produce some of the largest landslides observed on Earth (e.g., Moore et al., 1994; Harbitz et al., 2006; Oehler et al., 2008). The geohazards associated with such large landslides can sometimes include large tsunamis and destruction of undersea infrastructure (e.g., Harbitz et al., 2014; Carter et al., 2014). On many continental margins, submarine landslides occur repetitively and sometimes in a retrogressive nature, with head scarps migrating landward (Harbitz et al., 2006; Highland and Bobrowsky, 2008). The nature of landslide dynamics remains a subject of ongoing debate; some studies suggest rapid catastrophic failure (Watt et al., 2012; Cassidy et al., 2014), and others imply long-term creep (Le Friant et al., 2015; Hornbach et al., 2015). Understanding the physical properties of sediments where submarine slope failure occurs is fundamental to understanding sediment strength (Moscardelli et al., 2006; Madrussani et al., 2018). In particular, subsurface pore fluid pressure plays an important role in assessing slope failure hazards, as demonstrated in detailed land-based studies quantifying the relationship between rain, sediment permeability, and subsurface water pressure effects on slope stability (Terzsaghi et al., 1996; Hilley et al., 2004; Iverson, 2005). In

the marine environment, however, few permeability measurements exist in slope failure deposits, despite sediment permeability representing a fundamental physical property necessary for assessing and modeling submarine pore fluid pressure (e.g., Hornbach et al., 2015; Llopart et al., 2021).

It is currently hypothesized that the pore pressure gradient between nearshore low permeability hemipelagic sediments and high permeability turbidite deposits results in creeping slope failures. High accumulation rates of hemipelagic sediments near shore results in higher pore pressures in these sediments. This elevated pore pressure potentially leads to fluid movement downslope in the direction of higher permeability turbidite deposits. This fluid and pressure transfer is theorized to increase the possibility for mechanical failure in slope deposits (Hornbach et al., 2015). Testing this hypothesis, however, requires a better understanding of sediment permeability in the submarine environment. These data can be used to provide a better understanding of how permeability varies inside and outside slope failure deposits.

For this analysis, we chose an area of well-studied submarine landslides located offshore Montserrat and Martinique in the Lesser Antilles (Figure **F1**). These slides represent an ideal site to isolate and analyze sediment permeability in and around slope failures because (1) they consist of multiple well-dated slide events (Figure **F1**; Le Friant et al., 2015) that are easily distinguished in both high-resolution 2D and 3D seismic data; (2) the area has been extensively cored and drilled, including drilling during Integrated Ocean Drilling Program Expedition 340 and seafloor drilling using remote controlled Meeresboden-Bohrgerät (MeBo) drilling rigs attached to research vessels

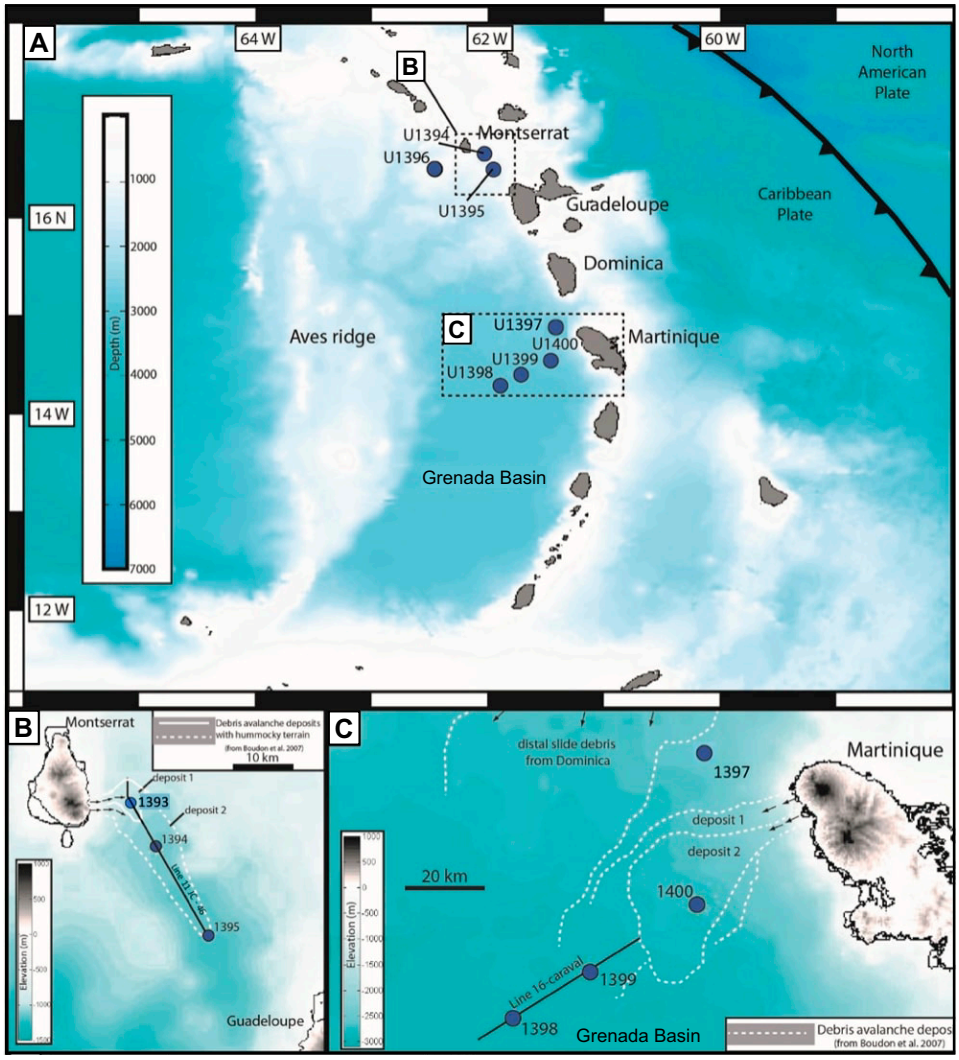

Figure F1. A–C. Bathymetry, Expedition 340 sites (adapted from Hornbach et al., 2015; Le Friant et al., 2015).

to recover sediment above, below, and within slope failures; and (3) there is evidence for both catastrophic and creep-like slope failure in the region associated with pore pressure evolution in the subsurface (e.g., Hornbach et al., 2015). Here, we focus on sediments in the upper 1 km of the seafloor that were drilled and cored during Expedition 340. These sediments include volcaniclastic turbidites and marine sediments inside and outside seismically identified submarine slides (Le Friant et al., 2015). In total, we measured permeability on 12 samples to assess changes above, below, and within slope deposits, as well as lateral variations in permeability within these deposits.

2. Materials and methods

2.1. Sample collection and preparation

The core samples used in this study were 10 cm^3 punch cores from sediments that were collected during Expedition 340 and stored at the Gulf Coast Repository at Texas A&M University (US). Dry samples were placed in the permeameters and rehydrated. The permeameters were then compressed as much as possible by hand before being fitted to the testing apparatus for measurements. This method is consistent with the approach used previously by Hornbach et al. (2015).

2.2. Core sample selection

A total of 12 core samples from 6 Integrated Ocean Drilling Program drill sites (U1393–U1395 and U1397–U1399) were selected in a guided effort to constrain permeabilities both inside and outside of landslide debris as well as changes in sediment permeability laterally along submarine landslides (Figure **F1**; Table **T1**). The selected sites contain sediments from several of the same seismically identified deposits but at varying locations downslope to allow interpretation of how permeability varies spatially (Figures **F2**, **F3**). Potentially overpressured sediments (Hornbach et al., 2015) (Samples 7

Table T1. Measured hydraulic conductivity and permeability values, Sites U1393–U1395 and U1397–U1399. **Download table in CSV format.**

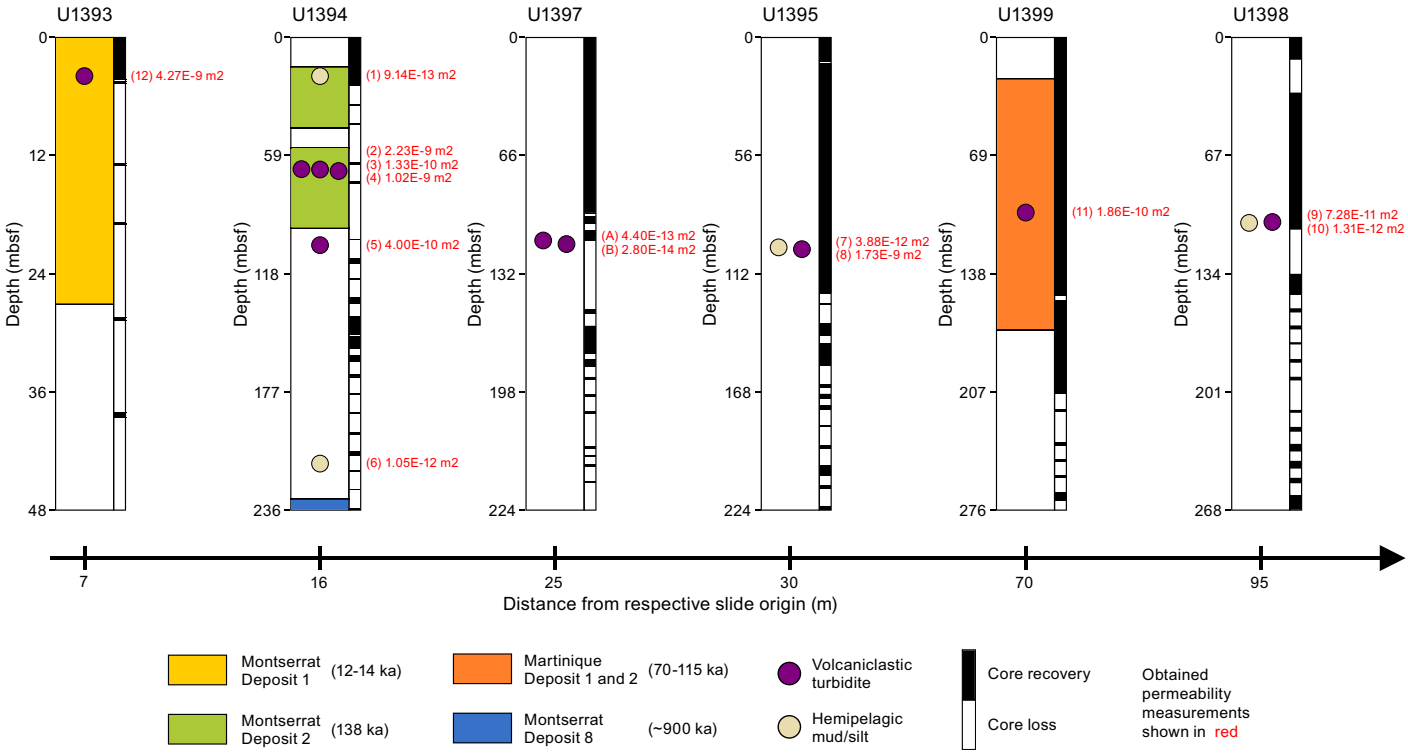

Figure F2. Approximate locations and ages of landslide deposits, core recovery, and selected samples, Sites U1393–U1395 and U1397–U1399. Samples A and B denote Site U1397 permeability values obtained from Hornbach et al. (2015).

and 8 [340-U1395B-11H-6, 10–12 cm, and 11H-6, 96–98 cm, respectively]) were also selected to assess if or how permeability relates to estimated elevated pore fluid pressure zones. Samples 1 and 5 (340-U1394B-3X-1, 50–52 cm, and 12H-6, 30–32 cm, respectively) were selected to constrain the upper and lower boundary permeabilities, respectively, of Montserrat Deposit 2. Samples 2, 3, and 4 (340-U1394B-8H-2, 14–16 cm, 8H-2, 32–34 cm, and 8H-2, 108–110 cm, respectively) represent volcaniclastic sands interbedded in landslide Deposit 2; these come from the landward portion of the slide adjacent to the headwall. Sample 6 (340-U1394A-24X-CC, 5–7 cm) represents the upper bounding layer of landslide Deposit 8, which is the oldest and deepest landslide unit identified by Le Friant et al. (2015). The aerial extant of landslide Deposit 8 is unknown at this time. Samples 7 and 8 were chosen because they might highlight changes in sediment permeability across a stratigraphic boundary at the downslope end of Montserrat Deposit 2. Samples 9 and 10 (340-U1398A-13H-3, 58–60 cm, and 13H-3, 108–110 cm, respectively) were chosen to assess permeability downslope of all known landslides offshore Martinique in a deepwater, low-energy environment and will be contrasted with Sample 11 (340-U1399A-13H-2, 55–57 cm) and previous measurements by Hornbach et al. (2015) that come from the toe of Deposits 1 and 2 offshore Martinique. Finally, Sample 12 (340-U1393A-1H-3, 7–9 cm) was obtained from the youngest, shallowest, and most landward slide deposit, located just below the headwall of Montserrat Deposit 1 (Le Friant et al., 2015).

2.3. Permeability measurement: the falling head method

In this study, we used the falling head method (Figure F4) to calculate the permeability of the selected sediments. Although experimental conditions are not equivalent to in situ conditions, measuring permeability in this manner is consistent with the falling head approach used in previous studies and therefore allows a consistent comparison with previous results at this site (Hornbach et al., 2015). This method uses a finite amount of water added to the permeameter. As the water flows through the sediment sample, water level (head) is measured over time. The gravity-driven flow rates are used to calculate the hydraulic conductivity (K) of the sediment and, in turn, the permeability (k). Darcy's law is used to describe these properties based on the dimensions of the sample and testing apparatus. The inner diameter of the falling head tube and the inner diameter of the sample chamber, as well as the length (L) of the sample in the tube, were measured for each apparatus. We secured the permeameters in place with clamps and allowed the feed end of the tubes to hang vertically with a small opening at the top, and the output end allowed water to drain. To maintain the sample in the

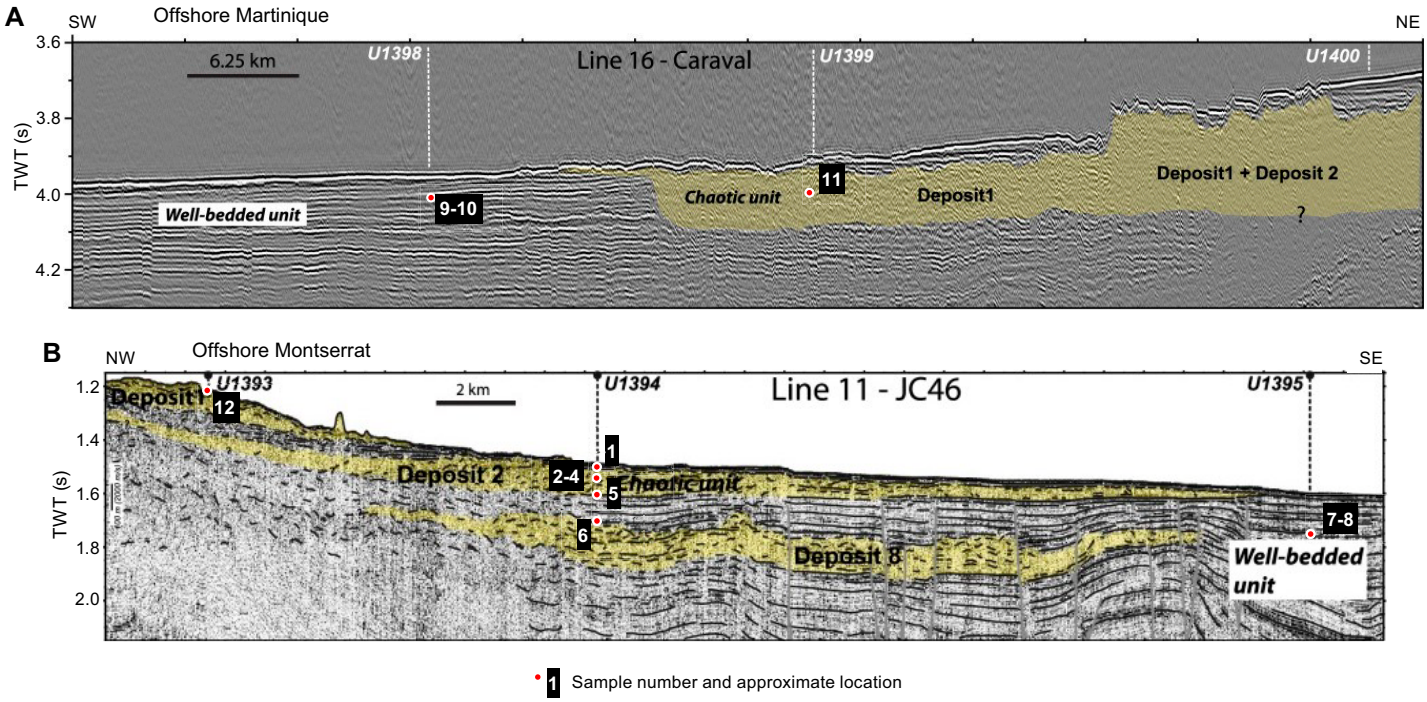

Figure F3. Approximate locations of selected core samples, Sites U1393–U1395, U1398, and U1399 (modified from Friant et al., 2015). TWT = two-way traveltime.

chamber, we used two layers of high permeability gauze on each end of the sample tube, connected these ends to the feed and output tubes with fittings, and then sealed each end to prevent leakage.

2.4. Measurements

Each sample was initially saturated. We then added water into the inflow end of the permeameters and measured the difference in the water level of the inflow tube and the outflow tubes over the course of hours and days. The change in water height over various time intervals was recorded and used to calculate hydraulic conductivity and permeability via the following relationships:

$$K = (L/t)\ln(h_0/h_t), \quad (1)$$

where

K = hydraulic conductivity (in meters per second),
L = length of the sample (in meters),
t = elapsed time (in seconds),
h_0 = initial head (in meters), and
h_t = head at the time of measurement (in meters).

The hydraulic conductivity can then be used to calculate the permeability of the sample:

$$k = K\mu/\rho g, \quad (2)$$

where

k = permeability (in square meters),
g = gravitational acceleration (9.8 m/s^2),
μ = dynamic viscosity of water at 25°C and 1 atm of pressure (8.9×10^{-4} Pa·s), and
ρ = density of water at 25°C and 1 atm of pressure (997 kg/m^3).

Ambient temperature during the experiments was kept between 21° and 24°C, and relative humidity remained between 30% and 40%. The evaporation rate of water in a stationary beaker adjacent to the experimental setup was measured and found to be less than 0.01 mm/day. Therefore, at this temperature and humidity, evaporation had negligible impact on the experiments. For all measurements, we conducted a double-blind approach, where each sample was measured in two different falling head apparatuses by different researchers to both constrain uncertainty and ensure consistency and reproducibility of results. These two apparatuses vary slightly with regard to the sample's length, diameter, and measured head and will be referred to as Setup A and B accordingly.

Permeability measurements were performed on 12 sediment samples from Expedition 340 Sites U1393–U1395, U1398, and U1399 (Table **T1**).

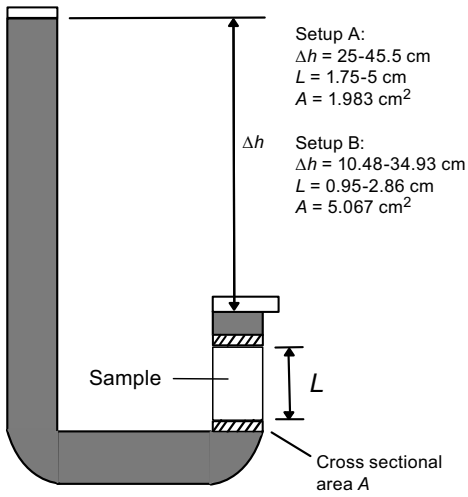

Figure F4. Schematic of falling head permeameter used for this experiment.

Table T2. Individual measurements, times, and calculated permeabilities for every trial of all samples, Sites U1393–U1395, U1398, and U1399. **Download table in CSV format.**

3. Results

The average permeability and hydraulic conductivity values for all samples are shown in Table **T1**. Some lower permeability samples (1, 7, 9, and 10) had high standard deviations resulting from variations in permeability across trials and setups. Low permeability samples had much smaller changes in head over time, increasing the chance of human error in measuring the head. Although the permeabilities of these samples are less accurate than the higher permeability sediments, these values still provide a useful order of magnitude approximation for the permeability of the hemipelagic muds. All measured heads, times, and calculated permeabilities are included in Table **T2**.

Results show generally consistent permeability values for sands ranging from E–11 to E–12 m^2. Values for hemipelagic muds ranged from E–14 to E–15 m^2. Although there are not enough data to constrain permeability patterns inside versus outside landslide deposits at this time, these permeability and conductivity values will assist future studies in the region.

4. Conclusions

New permeability measurements of submarine slope failures help constrain the permeability of submarine sediments associated with volcanic flank collapse in the Lesser Antilles arc. Collapse events offshore Montserrat show large erosional events and slope failures recorded in the sediment layers that showcase several slope failures overlain by hemipelagic sediment (Watt et al., 2012). The variation of permeabilities between sediment located within a slide deposit compared to adjacent sediment highlights an important connection between repeated failure events and possibilities for overpressure by overconsolidation. This study provides permeability values for samples collected within and adjacent to these landslide deposits and will assist future studies in the region. Further studies of permeability, porosity, and fluid flow in submarine sediments associated with landslides will help characterize the potential risk of tsunamis associated with these types of sediments.

5. Acknowledgments

This research used samples provided by the International Ocean Discovery Program (IODP). Funding for this research was provided by Southern Methodist University's Huffington Department of Earth Sciences and the Institute for the Study of Earth and Man. Special thanks to Dr. Katerina Petronotis at Texas A&M University for her help facilitating core sample selection, transportation, and logistics for this study.

References

Boudon, G., Le Friant, A., Komorowski, J.-C., Deplus, C., and Semet, M.P., 2007. Volcano flank instability in the Lesser Antilles Arc: diversity of scale, processes, and temporal recurrence. Journal of Geophysical Research: Solid Earth, 112(B8):B08205. **https://doi.org/10.1029/2006JB004674**

Carter, L., Gavey, R., Talling, P.J., and Liu, J.T., 2014. Insights into submarine geohazards from breaks in subsea telecommunication cables. Oceanography, 27(2):58–67. **https://doi.org/10.5670/oceanog.2014.40**

Cassidy, M., Watt, S.F.L., Palmer, M.R., Trofimovs, J., Symons, W., Maclachlan, S.E., and Stinton, A.J., 2014. Construction of volcanic records from marine sediment cores: a review and case study (Montserrat, West Indies). Earth-Science Reviews, 138:137–155. **https://doi.org/10.1016/j.earscirev.2014.08.008**

Harbitz, C.B., Løvholt, F., Pedersen, G., and Masson, D.G., 2006. Mechanisms of tsunami generation by submarine landslides: a short review. Norwegian Journal of Geology, 86(3):255–264.

Harbitz, C.B., Løvholt, F., and Bungum, H., 2014. Submarine landslide tsunamis: how extreme and how likely? Natural Hazards, 72(3):1341–1374. **https://doi.org/10.1007/s11069-013-0681-3**

Highland, L.M., and Bobrowsky, P., 2008. The landslide handbook—a guide to understanding landslides. US Geological Survey Circular, 1325. **https://pubs.usgs.gov/circ/1325/pdf/C1325_508.pdf**

Hilley, G.E., Bürgmann, R., Ferretti, A., Novali, F., and Rocca, F., 2004. Dynamics of slow-moving landslides from permanent scatterer analysis. Science, 304(5679):1952–1955. **https://doi.org/10.1126/science.1098821**

Hornbach, M.J., Manga, M., Genecov, M., Valdez, R., Miller, P., Saffer, D., Adelstein, E., Lafuerza, S., Adachi, T., Breitkreuz, C., Jutzeler, M., Le Friant, A., Ishizuka, O., Morgan, S., Slagle, A., Talling, P.J., Fraass, A., Watt, S.F.L., Stroncik, N.A., Aljahdali, M., Boudon, G., Fujinawa, A., Hatfield, R., Kataoka, K., Maeno, F., Martinez-Colon, M., McCanta, M., Palmer, M., Stinton, A., Subramanyam, K.S.V., Tamura, Y., Villemant, B., Wall-Palmer, D., and Wang, F., 2015. Permeability and pressure measurements in Lesser Antilles submarine slides: evidence for pressure-driven slow-slip failure. Journal of Geophysical Research: Solid Earth, 120(12):7986–8011. **https://doi.org/10.1002/2015JB012061**

Iverson, R.M., 2005. Regulation of landslide motion by dilatancy and pore pressure feedback. Journal of Geophysical Research: Earth Surface, 110(F2):F02015. **https://doi.org/10.1029/2004JF000268**

Le Friant, A., Ishizuka, O., Boudon, G., Palmer, M.R., Talling, P.J., Villemant, B., Adachi, T., Aljahdali, M., Breitkreuz, C., Brunet, M., Caron, B., Coussens, M., Deplus, C., Endo, D., Feuillet, N., Fraas, A.J., Fujinawa, A., Hart, M.B., Hatfield, R.G., Hornbach, M., Jutzeler, M., Kataoka, K.S., Komorowski, J.C., Lebas, E., Lafuerza, S., Maeno, F., Manga, M., Martínez-Colón, M., McCanta, M., Morgan, S., Saito, T., Slagle, A., Sparks, S., Stinton, A., Stroncik, N., Subramanyam, K.S.V., Tamura, Y., Trofimovs, J., Voight, B., Wall-Palmer, D., Wang, F., and Watt, S.F.L., 2015. Submarine record of volcanic island construction and collapse in the Lesser Antilles arc: first scientific drilling of submarine volcanic island landslides by IODP Expedition 340. Geochemistry, Geophysics, Geosystems, 16(2):420–442. **https://doi.org/10.1002/2014GC005652**

Llopart, J., Lafuerza, S., Le Friant, A., Urgeles, R., and Watremez, L., 2021. Long-term and long-distance deformation in submarine volcanoclastic sediments: coupling of hydrogeology and debris avalanche emplacement off W Martinique Island. Basin Research, 33(4):2179–2201. **https://doi.org/10.1111/bre.12553**

Madrussani, G., Rossi, G., Rebesco, M., Picotti, S., Urgeles, R., and Llopart, J., 2018. Sediment properties in submarine mass-transport deposits using seismic and rock-physics off NW Barents Sea. Marine Geology, 402:264–278. **https://doi.org/10.1016/j.margeo.2017.11.013**

Moore, J.G., Normark, W.R., and Holcomb, R.T., 1994. Giant Hawaiian landslides. Annual Review of Earth and Planetary Sciences, 22(1):119–144. **https://doi.org/10.1146/annurev.ea.22.050194.001003**

Moscardelli, L., Wood, L., and Mann, P., 2006. Mass-transport complexes and associated processes in the offshore area of Trinidad and Venezuela. AAPG Bulletin, 90(7):1059–1088. **https://doi.org/10.1306/02210605052**

Oehler, J.-F., Lénat, J.-F., and Labazuy, P., 2008. Growth and collapse of the Reunion Island volcanoes. Bulletin of Volcanology, 70(6):717–742. **https://doi.org/10.1007/s00445-007-0163-0**

Terzsaghi, K., Peck, R.B., and Mesri, G., 1996. Soil Mechanics in Engineering Practice: New York (Wiley).

Watt, S.F.L., Talling, P.J., Vardy, M.E., Masson, D.G., Henstock, T.J., Hühnerbach, V., Minshull, T.A., Urlaub, M., Lebas, E., Le Friant, A., Berndt, C., Crutchley, G.J., and Karstens, J., 2012. Widespread and progressive seafloor-sediment failure following volcanic debris avalanche emplacement: landslide dynamics and timing offshore Montserrat, Lesser Antilles. Marine Geology, 323–325:69–94. **https://doi.org/10.1016/j.margeo.2012.08.002**